International Symposium
On Turbulence and Shear Flow
Phenomena (TSFP-8)
August 28 - 30, 2013 Poitiers, France

DIRECT NUMERICAL SIMULATION OF TURBULENT FLOW WITH SUPERCRITICAL FLUID IN A HEATED PIPE

Hassan Nemati, Ashish Patel, Bendiks Jan Boersma, Rene Pecnik
Process and Energy Laboratory
Technische Universiteit Delft
Leeghwaterstraat 44, 2628CA Delft, Netherlands
r.pecnik@tudelft.nl

Abstract

This work investigates turbulent heat transfer to a pipe flow with a fluid close to its vapour-liquid critical point. The flow is simulated using Direct Numerical Simulations (DNS) of the anelastic Navier-Stokes equations at a Reynolds number of $Re_\tau = 360$, based on the friction velocity u_τ at the inlet and the diameter of the pipe. Turbulent statistics for two cases with forced and mixed convection are discussed. A decrease in turbulent kinetic energy is observed for both cases due to flow acceleration and buoyancy effects. Furthermore it is observed that the correlation between turbulent heat flux and Reynolds stresses is lower than in subcritical flows.

Introduction

Fluids close to their thermodynamic vapour-liquid critical point, also called supercritical fluids, have triggered interest in engineering applications, such as solvents in extraction processes, fossil fuel fired steam generators, nuclear reactors, transpiration cooling and convection cooling in rocket thrust chambers, etc. A supercritical fluid is a substance at a temperature and pressure above its critical point, where distinct liquid and gas phases do not exist. Close to the critical point small changes in pressure or temperature result in large changes in density, dynamic viscosity, specific heat and conductivity (Fig. 1). Owing to these characteristics, physical phenomena related to turbulent flows are not well understood. For instance, experimental and numerical studies showed that turbulent heat transfer to supercritical fluids can exhibit heat transfer deterioration or enhancement, which is the presence of minima and maxima in heat transfer coefficients along a heated surface.

Yamagata et al. (1972) showed in their experiments that for low heat to mass flux ratios heat transfer is enhanced close to the critical point. He further reported heat transfer deterioration for high heat to mass flux ratios. Kurganov and Kaptilnyi (1993) provided experimental data on flow structure, heat transfer, and hydraulic drag of supercritical (CO_2), heated in a vertical tube flowing upward and downward at very high Reynolds numbers. They found that the development of the M-shaped velocity profile due to buoyancy in upward flows favours the recovery of heat transfer deterioration. The ability of turbulence models to accurately predict the heat transfer characteristic is poor (He et al., 2008) and therefore DNS can help in better understanding the mechanisms involved in supercritical heat transfer. Earlier work on DNS of supercritical fluids were carried out by Bae et al. (2005, 2008). Their work has been taken as a reference for the development of the present work.

The goal is to simulate turbulent heat transfer in pipe flows, such that the pseudo-critical temperature T_{PC} is contained between the wall T_w and the bulk temperatures T_b; $T_w > T_{PC} > T_b$. Two different cases were performed and turbulent statistics are analysed and discussed in detail.

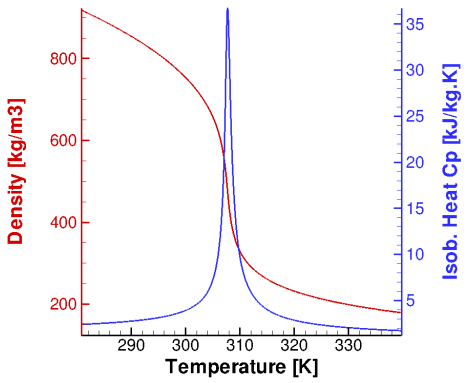

(a) Density and isobaric heat capacity

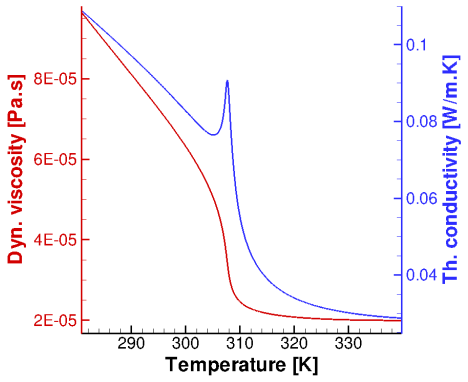

(b) Viscosity and thermal conductivity

Figure 1. Variation of thermophysical properties based on Span and Wagner (2003a,b) of carbon-dioxide (CO_2) vs. temperature at P_0 = 80 bar. The peak of the heat capacity at constant pressure indicates the location of the pseudo-critical temperature T_{PC}.

Governing equations and numerical method

In the present study the anelastic, respectively the low Mach number approximation, Navier-Stokes equations are solved to simulate a flow in a pipe slightly above the supercritical condition. Compared to solving the fully compressible Navier-Stokes equations, the solution of the anelastic Navier-Stokes equations circumvents the severe time step restrictions due to the small time scales of the acoustic waves. Additionally, ignoring compressibility effects and splitting the pressure field into its thermodynamic (P_0) and hydrodynamic part ($p(x,t)$) one can determine all thermodynamic state variables, such as density, enthalpy, etc., independently of the hydrodynamic pressure variations (Bae et al., 2005). Under these assumptions, the governing equations for mass, momentum and energy, can be expressed in dimensionless form as:

$$\frac{\partial \rho^*}{\partial t^*} + \frac{\partial (\rho^* u_j^*)}{\partial x_j^*} = 0, \tag{1}$$

$$\frac{\partial (\rho^* u_i^*)}{\partial t^*} + \frac{\partial (\rho^* u_i^* u_j^*)}{\partial x_j^*} = -\frac{\partial p^*}{\partial x_i^*} + \frac{\partial \tau_{ij}}{\partial x_j^*} \mp \frac{1}{Fr}\delta_{3i}\rho^*, \tag{2}$$

$$\frac{\partial \rho^* h^*}{\partial t^*} + \frac{\partial \rho^* u_j^* h^*}{\partial x_j^*} = \frac{1}{Re_\tau Pr}\frac{\partial}{\partial x_j^*}\left(\frac{k^*}{c_p^*}\frac{\partial h^*}{\partial x_j^*}\right), \tag{3}$$

with the Kronecker delta

$$\delta_{ij} = \begin{cases} i = j & 0 \\ i \neq j & 1 \end{cases} \tag{4}$$

and the shear stress tensor

$$\tau_{ij} = \frac{\mu^*}{Re_\tau}\left(\left(\frac{\partial u_i^*}{\partial x_j^*} + \frac{\partial u_j^*}{\partial x_i^*}\right) - \frac{2}{3}\delta_{ij}\frac{\partial u_k^*}{\partial x_k^*}\right). \tag{5}$$

The superscript * denotes non-dimensional quantities

$$x_i^* = \frac{x_i}{D}, \quad t^* = \frac{t}{D/u_\tau}, \quad u_i^* = \frac{u_i}{u_\tau}, \quad p^* = \frac{p}{\rho_0 u_\tau^2},$$

$$\rho^* = \frac{\rho}{\rho_0}, \quad k^* = \frac{k}{k_0}, \quad c_p^* = \frac{c_p}{c_{p0}}, \quad \mu^* = \frac{\mu}{\mu_0},$$

$$h^* = \frac{h - h_0}{c_{p0} T_0}, \quad T^* = \frac{T}{T_0}, \quad Q^* = \frac{q_w D}{k_0 T_0} = q^* Re_\tau Pr_0$$

$$Re_\tau = \frac{\rho_0 u_\tau D}{\mu_0}, \quad Pr_0 = \frac{\mu_0 c_{p0}}{k_0},$$

$$\frac{1}{Fr} = \frac{gD}{u_\tau^2} = \frac{Gr}{\beta_0 T_0 Re_\tau^2 Q^*}, \quad Gr = \frac{\rho_0^2 g \beta_0 q_w D^4}{\mu_0^2 k_0}, \tag{6}$$

where the subscript 0 refers to the inlet condition, u_τ is friction velocity, q_w is the constant heat flux, Gr is Grashof number, and D is the pipe diameter. In the momentum equation $\mp$ indicates the flow direction, minus sign for upward and plus for downward flow.

The equations (1)-(3) are solved using a staggered arrangement of the velocity components with respect to scalars in both space and time as shown in Fig. 2. A second order central difference scheme is used to discretize the spatial derivatives. The Koren (1993) slope limiter is used for the convection term in the energy equation to reduce oscillations due to sharp gradients. Spatial derivatives in circumferential direction for all diffusive terms are treated implicitly, while all the other terms are discretized explicitly. Adams-Bashforth time integration is used for the explicit part of the momentum equation and Crank-Nicolson for the implicit ones.

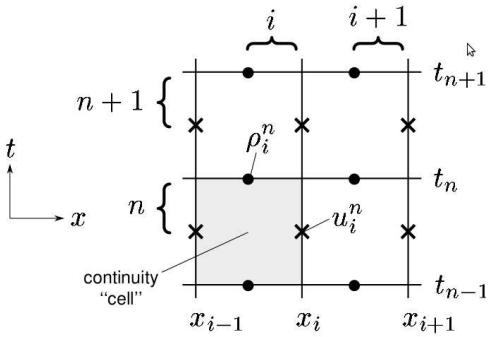

Figure 2. Staggered space-time grid (Pierce and Moin, 2004).

Geometry and boundary conditions

The simulation set-up consists of two parts. A periodic adiabatic pipe flow simulation is used to generate the inflow conditions for the developing pipe with constant wall heat flux (Fig. 3). Table 1 summarizes the flow conditions for the the cases with forced and the mixed convection for upward flow. For both cases the inflow conditions correspond to $P_0 = 80$ bar and $T_0 = 301.15$ K as given in Bae et al. (2005).

The inflow profiles required for the developing pipe flow are extracted from a periodic pipe simulation with $L/D = 5$. The mesh resolution for the inflow generator is 96x128x256 along the radial, circumferential and axial di-

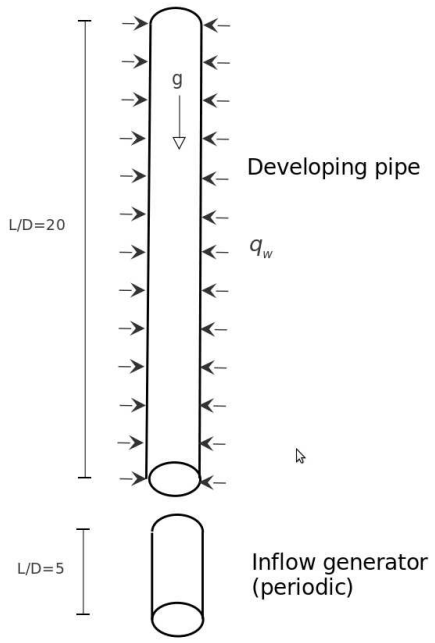

Figure 3. Geometry of the simulation domains.

Table 1. Flow conditions

Case	Type	Dir.	Re_τ	Pr_0	Gr^*	Q^*
A	Forced	-	360	3.19	0	2.4
B	Mixed	Up	360	3.19	21e6	2.4

rection, respectively.

Figure 4 compares the mean velocity profile and the root-mean-square velocity fluctuations for the periodic pipe simulation with the DNS data from Eggels et al. (1994). The mean velocity distributions are in good agreement with the Eggels data, while a slight disagreement is observed close to the centerline because of the coarser mesh in the current simulations in the core of the pipe. However, the mesh resolution is finer close to the wall in order to resolve the strong property variations due to the high temperature gradients.

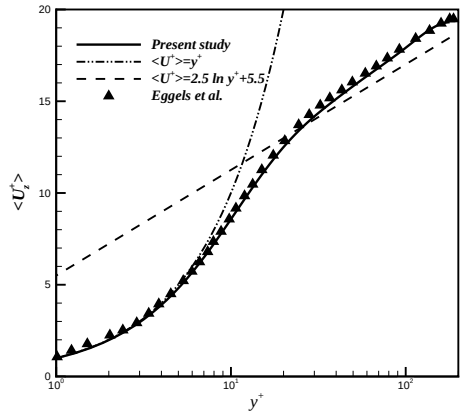

(a) Mean velocity profile

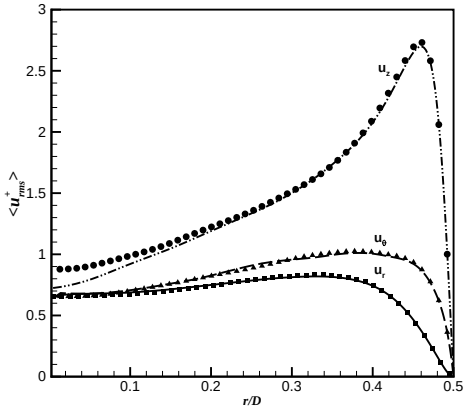

(b) Root-mean-square velocity fluctuations. Symbols: Eggels et al. (1994), lines present study.

Figure 4. Results for the periodic pipe flow (inflow generator) simulation.

Developing pipe results

The mesh resolution for the developing pipe with $L/D = 20$ is 96x128x512 along the radial, circumferential and axial direction, respectively. The mean quantities are calculated by taking an average over time and the circumferential direction. Two methods of averaging, namely Reynolds and Favre averaging, are used to present the results. $< \phi >$ denotes the mean of ϕ using Reynolds averaging, the fluctuation about this mean is denoted by ϕ'. Favre averaged mean $\tilde{\phi}$ and its fluctuation ϕ'', are defined as $\phi = \tilde{\phi} + \phi''$ with $\tilde{\phi} = \frac{<\rho\phi>}{<\rho>}$. The non-dimensional subscript * is dropped in further discussions for the sake of brevity.

The bulk mass flux G_b, bulk velocity U_b and bulk enthalpy H_b are defined based on mass and energy conservation as follows:

$$G_b = \frac{1}{A}\int < \rho U_x > dA, \quad H_b = \frac{1}{G_b A}\int < \rho U_x h > dA,$$
$$\rho_b = \rho(P_0, H_b), \quad U_b = \frac{G_b}{\rho_b} \tag{7}$$

Figure 5(a) shows the comparison of the streamwise bulk enthalpy H_b with the analytic solution obtained from the global energy balance, given as:

$$H_b = \frac{4Q^*}{Re_0 Pr_0}\frac{L}{D}, \tag{8}$$

with Re_0 the Reynolds number based on the bulk velocity and diameter. The comparison of the bulk velocity with data from Bae et al. (2005) is shown in Fig. 5(b). It shows a constant increase along the streamwise direction due to the decrease in the bulk density. Figure 5(c) shows the non-dimensional wall temperature for both flow conditions. The deviations between the data from Bae and the current simulations might be explained due to the different property data bases, different mesh resolutions and numerical schemes.

Figure 6 shows the turbulent kinetic energy, the turbulent kinetic energy production and turbulent shear stress for the forced (A) and the mixed (B) convection cases. The turbulent kinetic energy shows a decrease along the streamwise direction in Fig. 6(a). A similar decrease is observed for the turbulent production and turbulent shear stress in Fig. 6(b) and Fig. 6(c). For the forced convection the decrease in turbulence can be attributed to flow acceleration and to changes in the velocity profile. Similar observations were made by Kline et al. (1967). The velocity gradient increases close to the wall, where it has a small influence on turbulent production. On the other hand, the velocity gradient decreases further away from the wall, thus decreasing the turbulent production.

For the mixed convection case (B) the decrease in turbulence is amplified by buoyancy. Buoyancy has two effects, firstly it results in redistributing the Reynold stresses (due to body forces and changes in the velocity profile), secondly it alters the turbulent kinetic energy production by means of the gravity production term in the turbulent kinetic energy equation. The result showed that the second effect is small for this case and it is therefore not reported herein. However, it is important for cases with higher buoyancy. It should be mentioned that for upward flows buoyancy plays an interesting role. Its effect can result in both, deterioration and recovery depending on the amount of buoyancy.

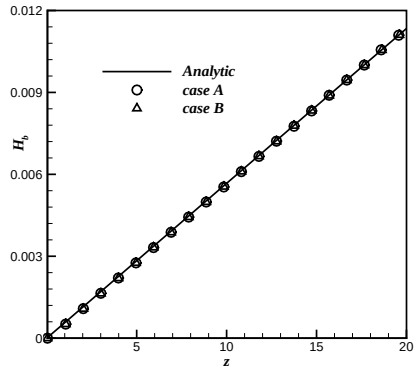

(a) Bulk enthalpy

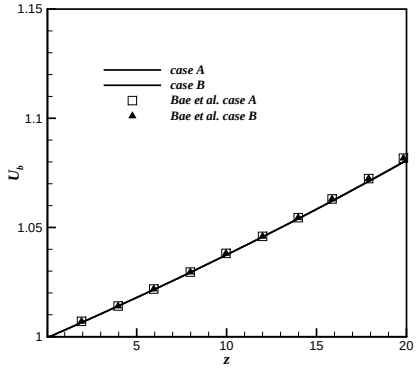

(b) Bulk velocity

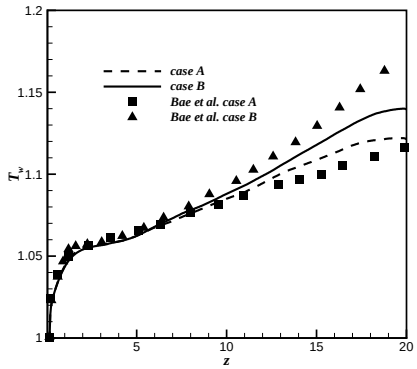

(c) Wall temperature

Figure 5. Bulk quantities and wall temperature in streamwise direction compared to data from Bae et al. (2005) and analytic solutions where available.

Figure 7 shows the profiles of $< \rho u_r'' h'' >$, $< \rho u_z'' h'' >$ and turbulent Prandtl number Pr_t for forced and mixed convection. Pr_t is commonly used in Reynolds averaged Navier-Stokes simulations (RANS) to model the turbulent diffusion term in the energy equation. It can be defined as $Pr_t = \frac{<\rho u_r'' u_z''>}{<\rho u_r'' h''>} \frac{\frac{\partial \tilde{h}}{\partial r}}{\frac{\partial \tilde{u}_x}{\partial r}}$.

The value of Pr_t within the viscous sublayer is of minor importance compared to the molecular diffusion. However, turbulent energy diffusion becomes more significant further away from the wall. The common practice in RANS is to use a constant turbulent Prandtl number. The reasoning behind the following assumption is that turbulent energy transfer is analogous to turbulent momentum transfer. This approach is also known as Reynold's analogy. As evident from Fig. 7(c) the turbulent Prandtl number shows a decrease at approximately $20 < y^+ < 30$. This might explain the fact why most turbulence model over predict the wall temperature. However further analysis is necessary and will be carried out in future. This breakdown between energy and momentum transfer is also evident by comparing $< \rho u_r'' u_z'' >$ in Fig. 6(c) and $< \rho u_r'' h'' >$ in Fig. 7(a). The comparison shows that the Reynolds shear stress $< \rho u_r'' u_z'' >$ decreases, while the peak of $< \rho u_r'' h'' >$ remains nearly constant. The decrease in turbulent Prandtl number is even more pronounced for the case with buoyancy.

The profile of $< \rho u_z'' h'' >$ in Fig 7(b) shows an increase in streamwise direction, but its derivative in streamwise direction is small and has a minor influence on the overall solution. However, it can play an important role in flows which undergo recovery as $< \rho u_z'' h'' >$ can change sign Bae et al. (2005). None of the results presented herein involves recovery and hence the role of this term will be analysed in future work.

Conclusion

A DNS of a heated pipe with a supercritical fluid was carried out for two different cases; one with a forced convection and one with mixed convection case. The results were compared for validation purposes to previously obtained data from Bae et al. (2005). Turbulent statistics were analysed and the results showed that flow acceleration and buoyancy affects the turbulent flow field and that the correlation between turbulent heat flux and turbulent shear stress cannot be modelled using a constant Prandtl number in RANS simulations.

REFERENCES

J.H. Bae, J.Y. Yoo, and H. Choi. Direct numerical simulation of turbulent supercritical flows with heat transfer. *Physics of Fluids*, 17(10), 2005.

J.H. Bae, J.Y. Yoo, and D.M. McEligot. Direct numerical simulation of heated CO2 flows at supercritical pressure in a vertical annulus at Re=8900. *Physics of Fluids*, 20 (5), 2008.

J. G. M. Eggels, F. Unger, M. H. Weiss, J. Westerweel, R. J. Adrian, R. Friedrich, and F. T. M. Nieuwstadt. Fully developed turbulent pipe flow: A comparison between direct numerical simulation and experiment. *Journal of Fluid Mechanics*, 268:175–209, 1994.

S. He, W. S. Kim, and J. H. Bae. Assessment of performance of turbulence models in predicting supercritical pressure heat transfer in a vertical tube. *International Journal of Heat and Mass Transfer*, 51(19-20):4659–4675, 2008.

S. J. Kline, W. C. Reynolds, F. A. Schraub, and P. W. Runstadler. Structure of turbulent boundary layers. *Journal of Fluid Mechanics*, 30:741–773, 1967.

B. Koren. *A Robust Upwind Discretization Method for Advection, Diffusion and Source Terms*. Afdeling Numerieke Wiskunde: Report NM. Centrum voor Wiskunde en Informatica, 1993.

V. A. Kurganov and A. G. Kaptilnyi. Flow structure and turbulent transport of a supercritical pressure fluid in a

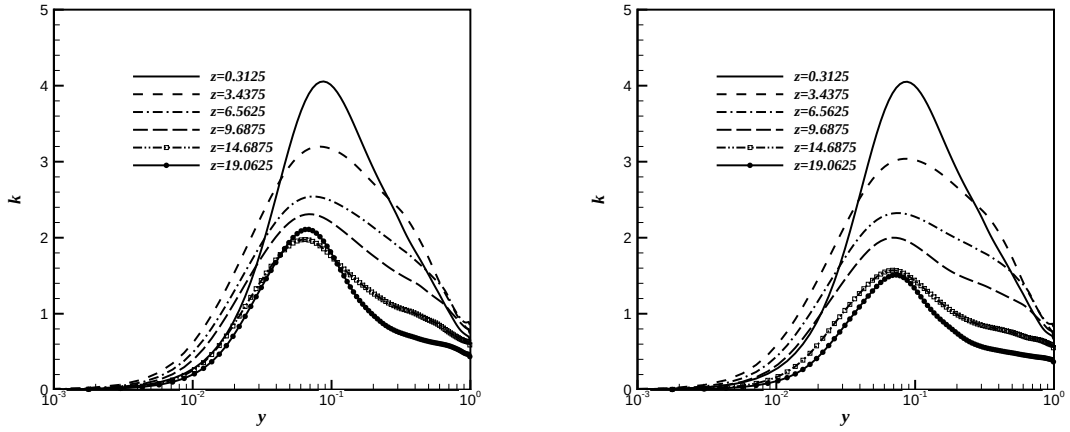

(a) Turbulent kinetic energy

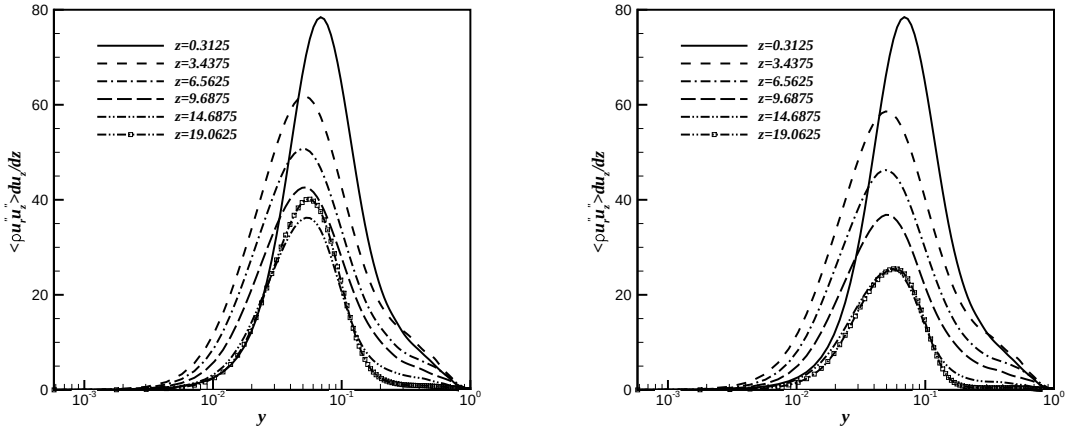

(b) Turbulent kinetic energy production

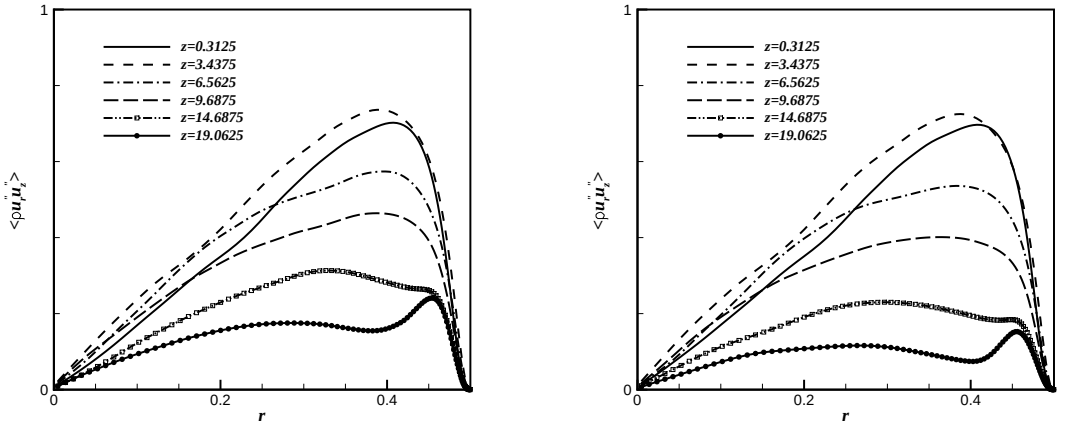

(c) Turbulent shear stress

Figure 6. Turbulent quantities at six different streamwise locations. Left column case A, right column case B.

vertical heated tube under the conditions of mixed convection. experimental data. *International Journal of Heat and Mass Transfer*, 36:3383–3392, 1993.

C. D. Pierce and P. Moin. Progress-variable approach for large-eddy simulation of non-premixed turbulent combustion. *Journal of Fluid Mechanics*, 504:73–97, 2004.

R. Span and W. Wagner. Equations of state for technical applications. I. Simultaneously optimized functional forms for nonpolar and polar fluids. *International Journal of Thermophysics*, 24:1–39, 2003a. ISSN 0195-928X.

R. Span and W. Wagner. Equations of state for technical applications. II. Results for nonpolar fluids. *Inter-*

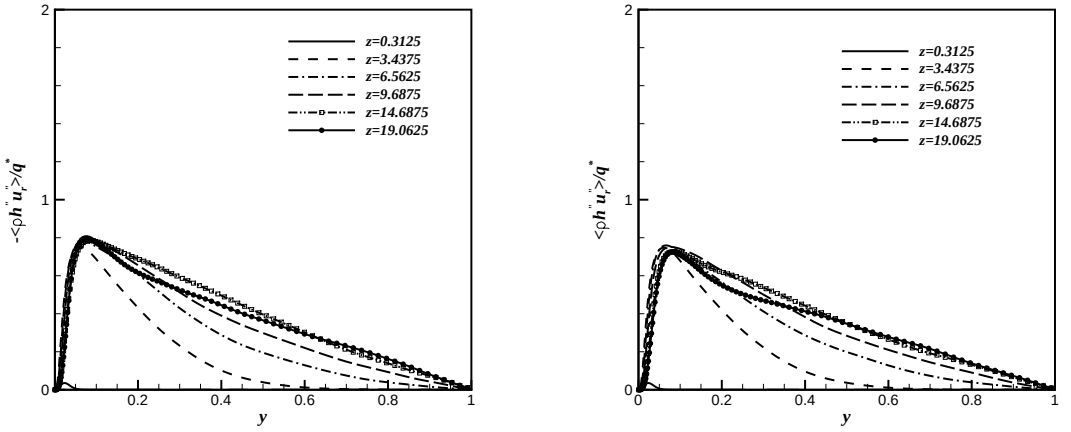

(a) Radial turbulent heat flux

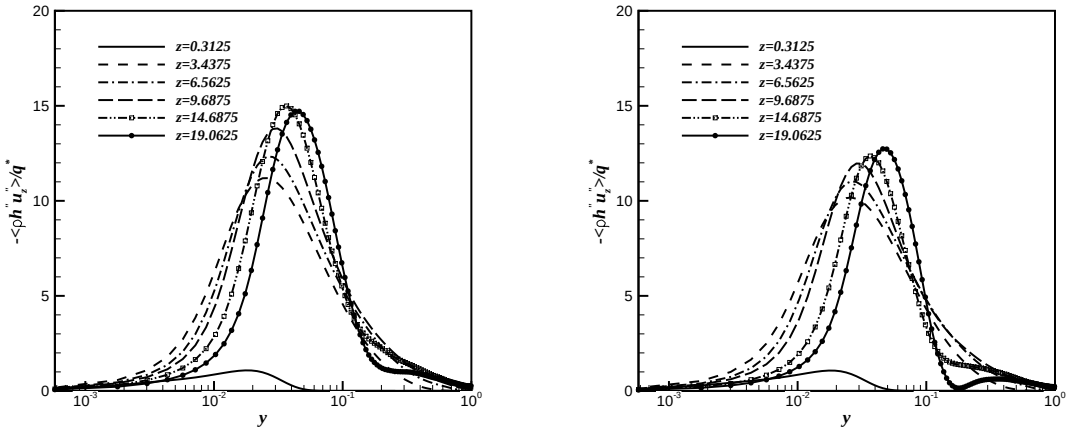

(b) Axial turbulent heat flux

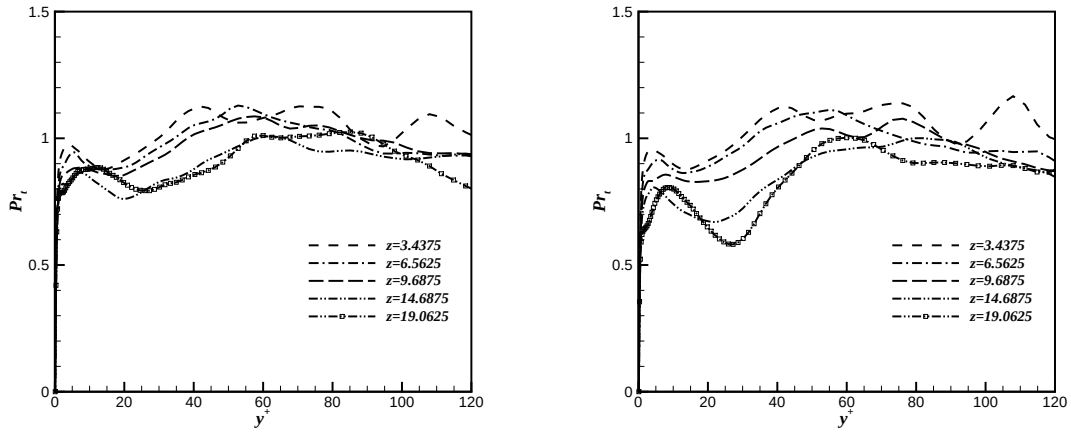

(c) Turbulent Prandtl number

Figure 7. Turbulent quantities related to the energy equation at six different streamwise locations. Left column case A, right column case B.

national Journal of Thermophysics, 24:41–109, 2003b. ISSN 0195-928X.

K. Yamagata, K. Nishikawa, S. Hasegawa, T. Fujii, and S. Yoshida. Forced convective heat transfer to supercritical water flowing in tubes. *International Journal of Heat and Mass Transfer*, 15:2575–2593, 1972.